Electrochimica Acta 338 (2020) 135866

Contents lists available at ScienceDirect

Electrochimica Acta

journal homepage: www.elsevier.com/locate/electacta

Changes in properties of scandia-stabilised ceria-doped zirconia ceramics caused by silver migration in the electric field

M. Mosiałek [a, *, 1], R.P. Socha [a], B. Bożek [a], D. Wilgocka-Ślęzak [a], E. Bielańska [a], A. Kežionis [b], T. Šalkus [b], E. Kazakevičius [b], A.F. Orliukas [b], M. Dziubaniuk [c], J. Wyrwa [c], J. Wojewoda-Budka [d], M. Faryna [d], B. Lis [e], M. Dudek [e, 1], R. Lach [c]

[a] Jerzy Haber Institute of Catalysis and Surface Chemistry, Polish Academy of Sciences, Niezapominajek 8, PL-30239, Krakow, Poland
[b] Institute of Applied Electrodynamics and Telecommunications, Faculty of Physics, Vilnius University, Sauletekio al. 9/3, 10222, Vilnius, Lithuania
[c] AGH–University of Science and Technology, Faculty of Material Science and Ceramics, Mickiewicza 30, Krakow, Poland
[d] Institute of Metallurgy and Materials Science Polish Academy of Sciences, 25 Reymonta St., 30–059, Krakow, Poland
[e] AGH–University of Science and Technology, Faculty of Energy and Fuels, Mickiewicza 30, Krakow, Poland

ARTICLE INFO

Article history:
Received 19 September 2019
Received in revised form
4 February 2020
Accepted 5 February 2020
Available online 9 February 2020

Keywords:
Scandia-stabilised ceria-doped zirconia
Low-energy electron microscopy
Solid oxide fuel cell
Broadband electrochemical impedance spectroscopy
High-temperature scanning electron microscopy

ABSTRACT

Silver is one of the most promising cathode materials for low temperature (300–500 °C) solid oxide fuel cells. The most important disadvantage of silver is its migration in the electric field. For better understanding of this phenomenon, an in situ observation of the migration mechanism was undertaken with the use of high-temperature microscopes. Scandia stabilised ceria doped zirconia CeScSZ electrolyte prepared from commercial powder was examined before and after silver migration experiments using scanning electron microscope. X-ray diffraction, broadband electrochemical impedance spectroscopy, and X-ray photoelectron spectroscopy. The silver electrodes for solid oxide fuel cells were prepared using magnetron sputtering. The described cells under polarisation were examined using a high-temperature low energy electron microscope. Reference cells and post-mortem cells were observed using a scanning electron microscope equipped with high temperature stage. Under polarisation, silver moved inside the electrolyte and along the surface towards the region between electrodes. The structures thus formed were similar to those previously described in the literature; however, direct observation of the deposit growth was unsuccessful. *In situ* scanning electron microscopy observations of the silver electrode at 650 °C revealed neither melting of the smallest silver particles nor movement of silver structures. Silver migration through the electrolyte caused a reduction in grain interior conductivity of the electrolyte, whereas its grain boundary conductivity remained unaffected.

1. Introduction

Research in the area of solid oxide fuel cells (SOFCs) is focused on devices operating in the intermediate temperature (IT) (500–700 °C) and low-temperature (LT) (300–500 °C) ranges. Pt and its alloys are considered to be the best cathode materials for LT-SOFCs operating at 300 °C because the high activation energy of the conductivity of strontium-doped perovskites – common cathode materials in the IT range results in their low performance in the LT range [1]. Kim et al. [1] demonstrated that a fuel cell with Ag-yttria-stabilised zirconia (YSZ) cathode achieved a peak power density of 100.3 mW cm^{-2} at 450 °C, which is 3–4 times higher than that obtained in similar cells with bare Ag or Pt cathodes. It was proved that silver is a valuable component of composite cathodes for SOFCs, improving their catalytic activity, electronic conductivity and, as a result the cell performance. A short review of literature concerning silver-containing electrodes was conducted in the previous work [2]. However, the most serious drawback of silver is the rapid displacement of Ag particles in the electric field, leading to the reductions in performance, the depletion silver in the composite cathode, and even the destruction of the cell [3–12]. Reported observations confirming the migration of silver at negatively polarised point electrodes include: (i) a rapid increase in current during chronoamperometry experiments; (ii) a decrease in resistance in EIS measurements, (iii) an inductive loop in cyclic

* Corresponding author.
E-mail addresses: nbmosial@cyfronet.pl, nbmosial@cyf-kr.edu.pl (M. Mosiałek).
[1] ISE member.

https://doi.org/10.1016/j.electacta.2020.135866

voltammograms; (iv) the appearance of silver deposits on the electrolyte surface around the electrode during experiments [3,8–12]. The problem of the electromigration of metal used as an electrode or electrode component material is very important in SOFCs, affecting almost all frequently used metals. Similar behaviour was reported in the cases of platinum, palladium, and gold [8,9,13,14], however, the scope of the present work is confined to silver.

Although research on the mechanism of silver migration was carried out in the last century, the problem was never solved or understood. This is an important phenomenon in terms the to design and elaboration of composite cathodes containing silver nanoparticles, revealing enhanced catalytic activity in the oxygen reduction within a temperature rangeof 500–700 °C (IT) compared to similar cathodes without silver. In some solutions, the advanced methods were applied in order to achieve special architectures of the cathode oxide matrix as well as silver particle distribution [15,16].

Some authors have explained Ag movement in the terms of transport in the form of gaseous oxides [8,9], although, the equilibrium vapour pressure of silver oxide, much lower when compared to that of silver [8] indicates that in a gas in thermodynamic equilibrium with solid silver, gaseous silver oxide decomposes into silver and oxygen. On the other hand, the rate of silver evaporation [11,17] does not explain such a huge amount of transported metal [11]. Another issue is the direction of silver transport from the cathode to the anode [3,5–13] which is opposite to the positive charge of the silver ion. Ho and Huntington [18] reported the migration of silver from the cathode to the anode and explained this direction of movement in the terms of the electron wind theory (EWT). The authors stated that the rate of silver transport is proportional to the current, however, the rate of the silver transport in SOFCs [10,11] compared to the flowing current is several orders of magnitude faster than could be expected on the basis of the EWT. The movement of silver along the electrolyte surface is suggested in Refs. [3,8,10–13]. The observation, reported by Raźniak et al. [9], that the migration of silver proceeds more rapidly at the well-polished surface of the electrolyte confirms this mechanism. The electromigration of silver along the surface of several ionic conductors has been reported for YSZ [10], lanthanum strontium manganite [10], samaria-doped ceria (SDC) [3,12] gadolinia-doped ceria (GDC) [11] and porous $(Bi_2O_3)_{0.8}(Er_2O_3)_{0.2}$ [5]. Another interesting finding was reported by Sasaki et al. [4] who described the electromigration of silver through the scandia-stabilised ceria-doped zirconia (CeScSZ) electrolyte and found metallic silver particles along grain boundaries in the anodic part of the electrolyte. The affected volume of the electrolyte was discernible due to a colour change from white to orange. These authors proved that the movement of silver through the electrolyte takes place in one direction only from the cathode to the anode.

In the IT range Scandia doped zirconia (ScSZ), SDC, and GDC reveal a much higher level of ionic conductivity than YSZ, however, stabilised zirconia unlike SDC and GDC, does not reveal electronic conductivity at the low oxygen partial pressures prevailing in the anode chamber. The cubic phase of ScSZ, which exhibits excellent ionic conductivity, is not stable at lower temperatures [19,20]. Kazlauskas et al. [20] observed the phase transition leading to the lower conductive rhombohedral phase at 561 and 513 °C during the heating and cooling cycle, respectively. ScSZ co-doped by an additional trivalent cation such as Ce, Sm, Yb, Al or Gd reveals greater cubic phase stability than pure ScSZ [21–25]. Dasari et al. [25] reported that an amount of ceria dopant as low as 0.5% is enough to suppress the undesirable phase transition.

CeScSZ, which seems to be the most promising electrolyte material for SOFCs and solid oxide electrolysis cell working in the IT range is supplied by several companies in industrial amounts. Accordingly, we decided to use one of the commercially available compounds that we had carefully characterised. In our investigations.

All of the above-mentioned works concerning the electromigration of silver [3–5,8–13] described the results of electrochemical measurements performed during electromigration experiments and microscopic observations performed after electromigration experiments. In the present work, we describe for the first time, microscopic observations of silver electrodes deposited on a CeScSZ electrolyte made in situ in the IT temperature range during electromigration, although the gas partial pressures and applied potential differed significantly from typical conditions in the cathode chamber of a working SOFC due to instrumental limitations.

2. Experimental

2.1. Electrolyte preparation and characterisation

CeScSZ powder described by the manufacturer (Terio Corporation., Qingdao, China) as 10ScCeSZ ($(Sc_2O_3)_{0.10}(CeO_2)_{0.01}(ZrO_2)_{0.89}$), was used for the preparation of ceramic electrolyte disks. A paste consisting of distilled water and the CeScSZ powder was isostatically pressed at a pressure of 12.75 kPa; pellets were then sintered at 1660 °C for 2 h. Dense electrolyte discs 20 mm in diameter with thickness in the range 0.95–1.0 mm as well as 3 mm diameter and the thickness in the range 1.5–1.55 mm, were obtained. The XRD measurements were performed using X'Pert Pro system and Empyrean X-ray diffractometer both manufactured by PANalytical. The measurements were performed using the monochromatic radiation with the wavelength corresponding to the K_α emission line of copper, within the 5–90° angle range in the 2θ scale, and with the goniometer step size of 0.008°. The qualitative analysis of the phase composition was performed using the X'Pert HighScore Plus software, version 3.0e, designed by PANalytical. To identify the phase composition, the obtained diffraction patterns were compared to the FIZ Karlsruhe 2012 powder diffraction database and to ICDD database (PDF-2 (2004) and PDF-4+(2019)). The Rietveld refinement method [26] was used to determine the cell parameters of the 10ScCeSZ crystallographic structure.

Microstructural observations of CeScSZ powder and discs were carried out using the JEOL JSM–7500 F scanning electron microscope with X-ray energy dispersive spectroscopy (EDS) (INCA PentaFetx3). The density of sintered CeScSZ pellets was measured using an AccuPyc 1340 (HP) Pycnometer (Micromeritics Instrument Corporation).

For EIS measurement, platinum electrodes were made by means of painting with 71% Pt (MaTeck) platinum conducting paste for brush application then firing at 400 °C for 1 h and at 700 °C for 20 min with a heating and cooling rate 1 °C min^{-1}. Two platinum electrodes at the tops and bottoms of cylinder samples were made in this manner, whereas at the postmortem sample four electrodes were made for 4-electrode setup as is illustrated in Fig. 2 in the previous work [2]. The electric conductivity of the CeScSZ samples was tested using a broadband impedance spectrometer [27] in the air in the 27–727 °C temperature range and in the $1–10^{10}$ Hz frequency range with logarithmic frequency steps of 54 points per decade. The AC signal amplitude was 100 mV at frequencies up to 2 MHz and ~200 mV at frequencies above 2 MHz. The Minuit program [28] was used for fitting. The data-treatment procedure is described in detail in Ref. [29].

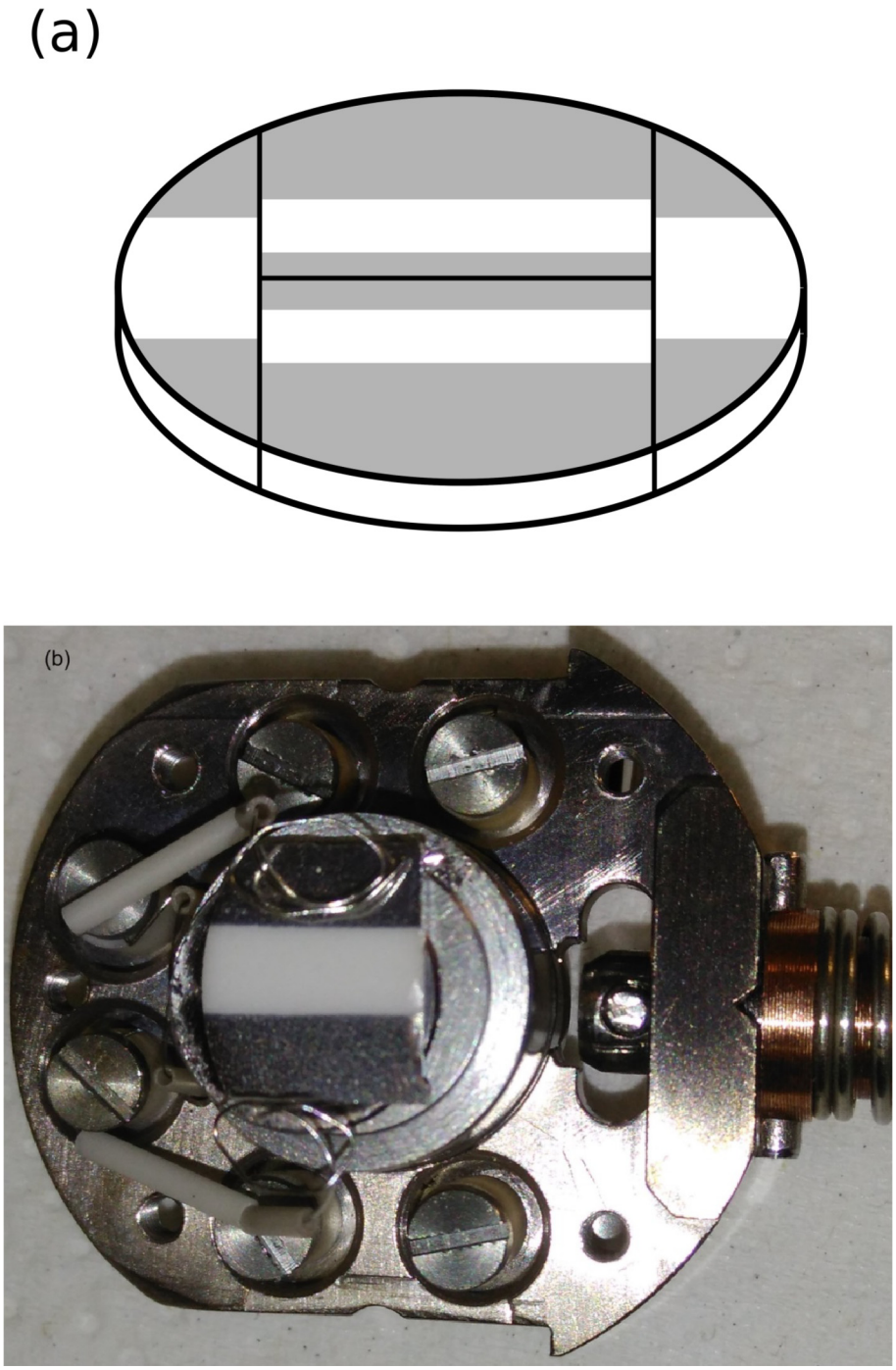

Fig. 1. Prepared cells for microscopy experiments, (a) an electrolyte disc 20 mm in diameter was cut along the black lines, silver electrodes were sputtered at the area coloured in grey, (b) mounted cell in the holder.

2.2. Examination of silver electrodes

Electrolyte disks were prepared for silver electrode examinations by means of polishing first using emery paper #1200, then a Struers Tegramin 20 in manual mode with an MD-Plan disc and 9 μm diamond slurry, followed by a 0.04 μm suspension of colloidal silica (OP—S, Sturers) at 300 rpm. The 20 mm discs were cut as shown in Fig. 1a, then the silver electrodes were deposited via the magnetron sputtering technique. The deposition system (MeasLine) contained a 2″magnetron, the deposition rate was controlled by a quartz crystal microbalance. The thickness of the deposited silver electrodes was 20 nm for a portion of the samples and 50 nm for the remainder. The gap between electrodes was 3 mm.

Surface properties of the electrolyte were investigated on the polished samples presented in Fig. 1 using low energy electron microscopy (LEEM), specifically model LEEM III (Elmitec). This microscope works under ultrahigh vacuum (UHV) conditions with a base pressure of 5×10^{-11} mbar. Prior to imaging, the sample was degassed for several hours at 600 °C. The sample holder in the microscope contained two special contacts connected to a power

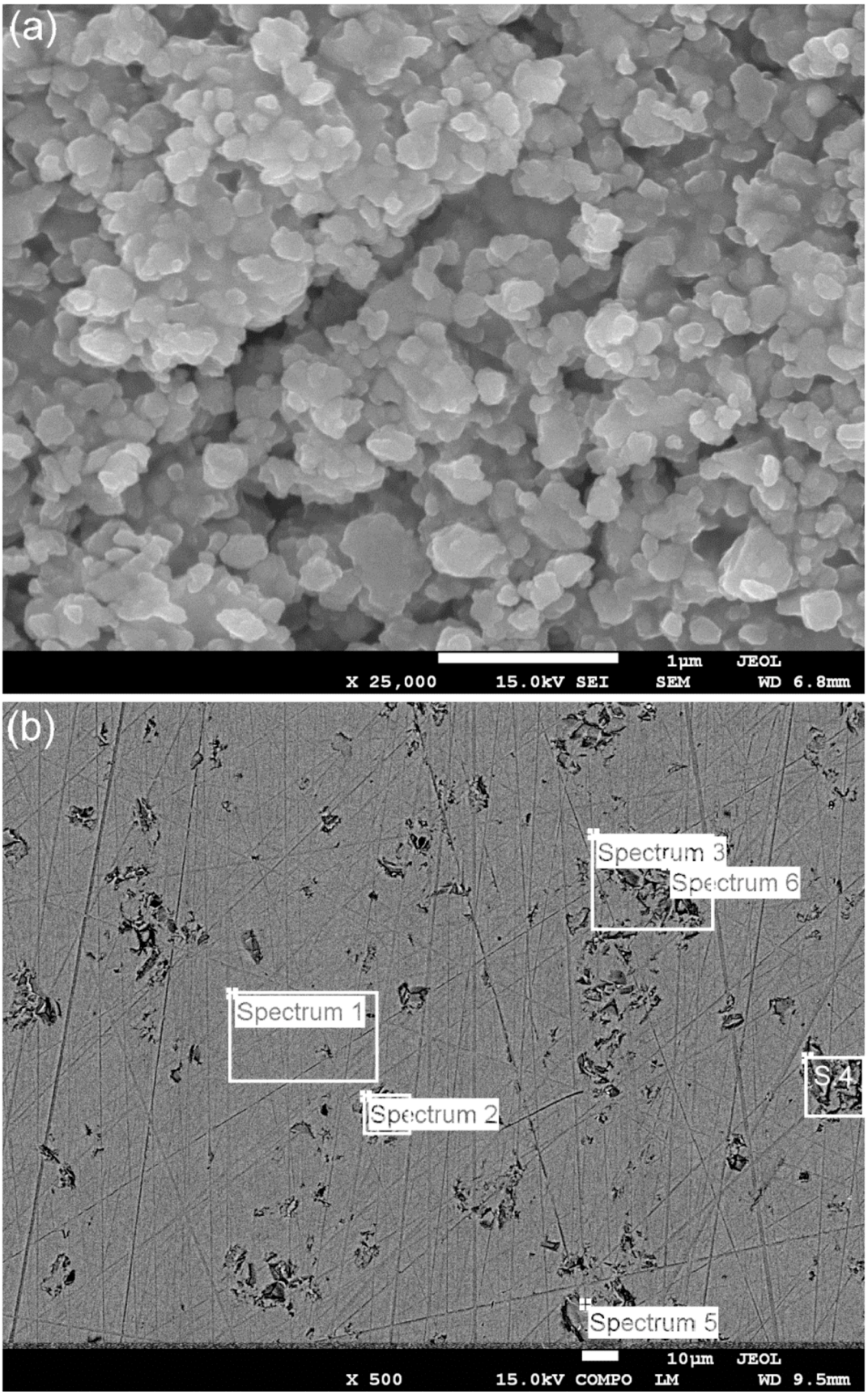

Fig. 2. SEM microphotograph of CeScSZ powder (a); the areas where EDS analyses were performed on the polished surface of the sintered disc (results are presented in Table 1) (b).

supply that enabled polarisation of the silver electrodes up to +/−12 V (Fig. 1b).

The surfaces of other cells i.e. untreated reference cells and cells after experiment performed in LEEM were examined using a dual beam FEI QUANTA 3D FEGSEM equipped with a GATAN Murano 525 heating stage with a UBS temperature controller. To record images of secondary electrons at elevated temperatures an Everhart-Thornley SE Detector was used. Neither backscattered electrons or vCD (low voltage high contrast) detectors were used due to the risk of heat damage. A working distance larger than 10 mm was chosen to prevent the aperture bullet from extensive heat. The set points at which the images were recorded were as follows: 225, 300, 450, 500, 550, 600 and 650 °C with 15 min soaking time to stabilise measuring conditions. An accelerating voltage of 15 kV and current of 16 nA were applied during the observations. Low-vacuum mode (0.45 Torr) was essential to apply in these observations. The scanning electron microscopy (SEM) observation of CeScSZ was performed for original reference samples. In these experiments, the surfaces of investigated samples were not covered by the conductive layers (gold, carbon, etc.) usually applied at the top of weakly conducting observed material.

The X-ray photoelectron spectroscopy (XPS) measurements were performed in an ultrahigh vacuum (3×10^{-10} mbar) system equipped with a hemispherical analyser (SES R 4000, Gammadata Scienta). The measurement system was calibrated according to ISO 15472:2010. The electron binding energy (BE) scale of the acquired spectra was calibrated for the maximum of C 1s core excitation at 285 eV. The analysis area was 3 mm^2. A similar procedure for XPS investigations of surface ceramic electrolytes such as YSZ and GDC before and after polarisation was described in previous papers [10,11].

3. Results and discussion

3.1. Characterisation of CeScSZ powder and sintered samples using scanning electron microscopy

SEM analyses (Fig. 2a) reveal that CeScSZ powder consists of 100 nm crystallites mostly combined into 0.5–1.5 μm aggregates (Fig. 1a). EDS measurements of the sintered and polished electrolyte sample taken from the area shown in Fig. 2b are presented in Table 1. Taking into account that EDS measurement error is about 1% and the accuracy of measurement of light elements (oxygen) is even smaller the overall formula of the examined sample should be written thus $Ce_{0.01}Sc_{0.18}Zr_{0.81}O_{1.91}$.

The microstructure and grain size distribution of sintered CeScSZ electrolyte sample is presented in Fig. 3.

The measured density of the sintered CeScSZ sample was equal to 5.716 ± 0.0034 g cm^{-3} which is 99,7% of the theoretical density equal to 5.732 g cm^3 for the formula $Ce_{0.01}Sc_{0.18}Zr_{0\cdot81}O_{1.91}$ found by EDS.

Table 1
Results of EDS analysis in at% of the samaria doping level measured in the areas shown in Fig. 2b

Spectrum	O	Sc	Zr	Ce
Spectrum 1	60.5	6.7	32.5	0.2
Spectrum 2	63.3	6.6	29.5	0.7
Spectrum 3	62.9	6.9	30	0.3
Spectrum 4	65.2	6.4	28	0.5
Spectrum 5	62.3	6.8	30.8	0.1
Spectrum 6	64.4	6.6	28.7	0.3
Mean	63.1	6.7	29.9	0.3
Std. deviation	1.6	0.2	1.6	0.2

3.2. X-ray diffraction investigation of sintered CeScSZ discs

The HT- XRD pattern recorded within the temperature range 25–800 °C for CeScSZ sintered electrolyte discs (Fig. 4) indicated that mainly cubic structure was observed for CeScSZ solid solutions. The coexistence of the tetragonal phase was found in the temperature range 350–400 °C. The variation of cell parameter a calculated for the CeScSZ sample sintered is presented in Fig. 4b. A linear increase in cell parameter *a* is observed within the temperature range 25–800 °C.

3.3. In situ observations of polarised cell using low energy electron microscope

Despite the huge charging effects of the sample related to the poor conductivity of the material it was possible to perform imaging at elevated temperatures (above 350 °C) using electrons with the energy values of approximately 14 eV and 35 eV. The typical LEEM image of the electrolyte surface are presented in Fig. 5, shows 2–10 μm sized grains that reveal the different level of contrast corresponding to differences in electron reflectivity. Diffraction patterns of low energetic electrons collected from individual grains (micro-LEED) (Fig. 5b–d) demonstrate their well-ordered, single-crystalline structure. Most of the grains observed on the surface reveal high symmetry patterns. The non-central and mutable position of the specular spot (00) in the particular LEED patterns indicates that surfaces of grains are slightly misaligned in respect one to another as well as in respect to the net surface. Regular, straight grain-walls with characteristic directions that are oriented mutually under 120° or 90° or 60° suggest that the crystallites expose high symmetry planes.

During LEEM imaging performed at the CeScSZ electrolyte surface, the cell was polarised applying a 12 V bias between silver electrodes. Imaging condition relies on the applied bias. During experiments we did not observe changes caused by moving silver, however, after experiments, we found changes in the morphology of examined samples.

Short-time breaks in the polarizations caused immediately 50 times decreases in the overall gas pressure in the microscope chamber.

3.4. Postmortem observations of Ag|CeScSZ|Ag cell

Fig. 6a shows the 20 nm thick silver electrode before the experiment, whereas the cell with silver electrodes after 162 min 12 V polarisation at 540 °C in LEEM at 2×10^{-8} mbar is presented in Fig. 6b. The CeScSZ electrolyte is yellow in comparison to Al_2O_3 insulators (Fig. 6b). The electrode side of the cell (Fig. 6c,e) reveals that silver almost vanished from the negatively polarised electrode (cathode) (left in Fig. 6c), whereas at the anode (right electrode in Fig. 6c) silver layer is thick. The intensive red colour observed at the right and upper part of the cell (Fig. 6c) as well as the upper and left part of the rear side of the cell (Fig. 6d) is present in the whole bulk of the electrolyte. This sample was polarised by 12 V bias by 162 min whereas in experiments described by Sasaki et al. [4] lasted for 168 h, only a part of the electrolyte thickness was coloured in orange. However, in our experiments, the applied bias was one order of magnitude larger. The not uniform shape of the coloured part of the electrolyte points that there was not the same current density along the electrode border. The current collector steel wires contacted the silver layer in a quasi-point small area. At the cathode side, the silver is much thinner than after sputtering and is practically depleted around the place, where the steel wire contacted electrode (Fig. 6e). At the anode side, the silver layer is thick and near the places where steel current collector contacted electrode,

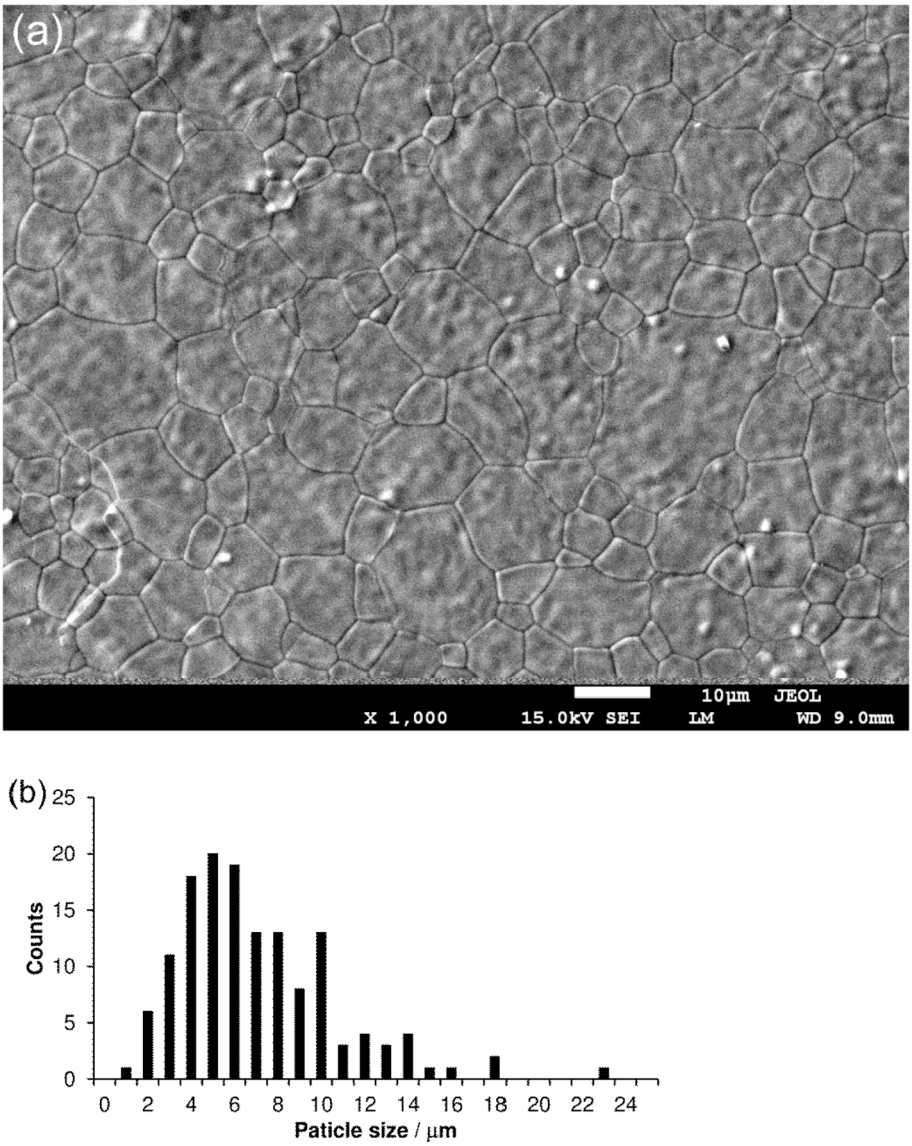

Fig. 3. The surface of the sintered electrolyte (a); particle size distribution (b).

the blue coloured area is observed (Fig. 6f), whereas in another experiment, where silver current collector wires were used, the blue area was not observed.

The careful examination was performed at the postmortem cell as is shown in Fig. 7.

The changes in the morphology of the silver electrodes and the electrolyte surface were performed at the area in rectangle "1". The part of the opposite to electrodes surface sample was examined by XPS on the rectangle part of the surface "2". The cuboid sample was cut-off from the intensively coloured border "3", cleaned and polished by emery paper, Four platinum electrodes were deposited for 4-electrode setup as is illustrated in Fig. 2 in the previous work [2], then the broadband IS measurement was performed. The cross-section of the sample was made along the line "4–5" and examined by SEM.

3.5. Post-mortem SEM observations of the surface of Ag|CeScSZ|Ag cell

The surface of the cell was examined using scanning electron microscopy (Fig. 8). The EDS analysis confirmed that the bright area was composed of silver, whereas in the darker area zirconium scandium and cerium were present. The general view of the electrolyte surface under lower magnification showed the electrolyte surface and two borders of silver electrodes. The left border was characterised by a rather planar shape (Fig. 8a) whereas the other was irregular (wavy) (Fig. 8b).

The dense silver layer visible in the left part of Fig. 8a is separated from the bare electrolyte surface by an area covered by silver particles characterised by droplet shapes which arose on both the electrode and the electrolyte surface (Fig. 8c). Closer to the central part of the cell, the silver droplets became smaller and smaller, and distances between them greater and greater (Fig. 8d). Tiny single particles of silver were detected as far as 250 µm from the border 1. The irregular (wavy) border seen at higher magnifications revealed a much larger area of covered electrolyte surface (Fig. 8e) and some larger silver cathode fragments that remain after polarisation (Fig. 8f). These deposits were similar to those previously described on the near electrode surfaces of the GDC [11] and SDC [3,12] electrolytes. Single cracks seen on this substrate surface were

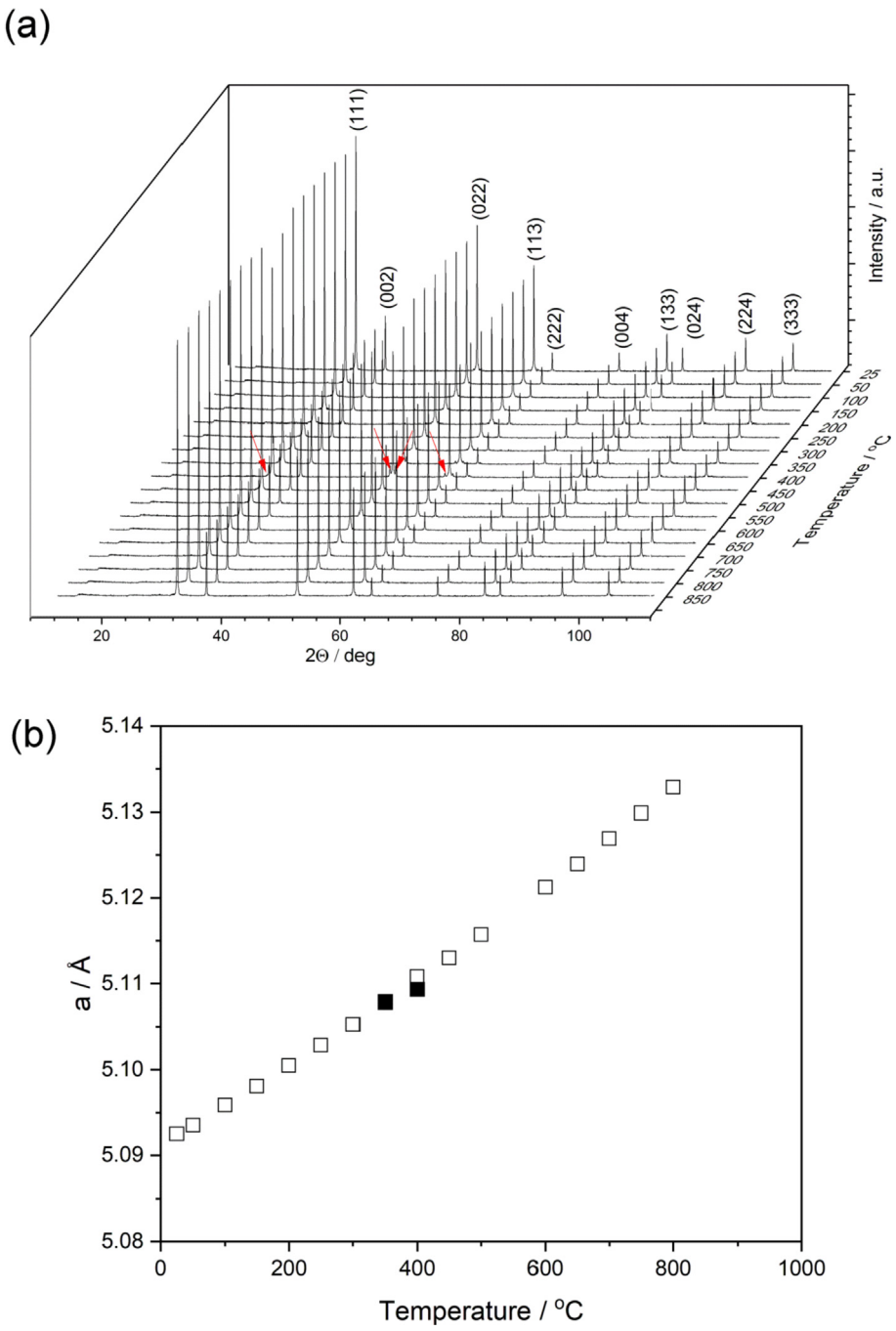

Fig. 4. The HT-XRD pattern recorded for CeScSZ samples within the temperature range 25–800 °C (a); variation in cell parameter of CeScSZ within the temperature range 25–800 °C in the heating-cooling cycle (b). The empty squares presented values calculated considering only the cubic phase whereas filled squares the cubic and the tetragonal phase.

directly caused by applied experimental conditions. The cooling rate exceeded 50 °C min^{-1}. Other samples cooled slowly at 10 °C min^{-1} remained free of cracks.

The SEM examinations of the cross-section did not found the silver crystallites at the grain boundaries, whereas EDS analysis found some silver in the amount not exceeding 0.24 at%.

3.6. High-temperature SEM without polarisation

In order to document our observations related to the migration of silver in the electrolyte at temperatures of 25–650 °C under the influence of polarisation, another experiment was carried out, confirming that the observed phenomena were affected only by polarisation, to a lesser extent by temperature. Changes in the electrolyte were observed in a cell polarised in a vacuum within a wide temperature range. The similar cell was observed in the 275–650 °C temperature range using a FEGSEM microscope without polarisation to distinguish the potential influence of temperature on the silver migration process.

SEM images of the border of the silver electrode are shown in Fig. 9. The surface of CeScSZ electrolyte is visible in the whole area of the presented picture whereas in the bottom half of the picture

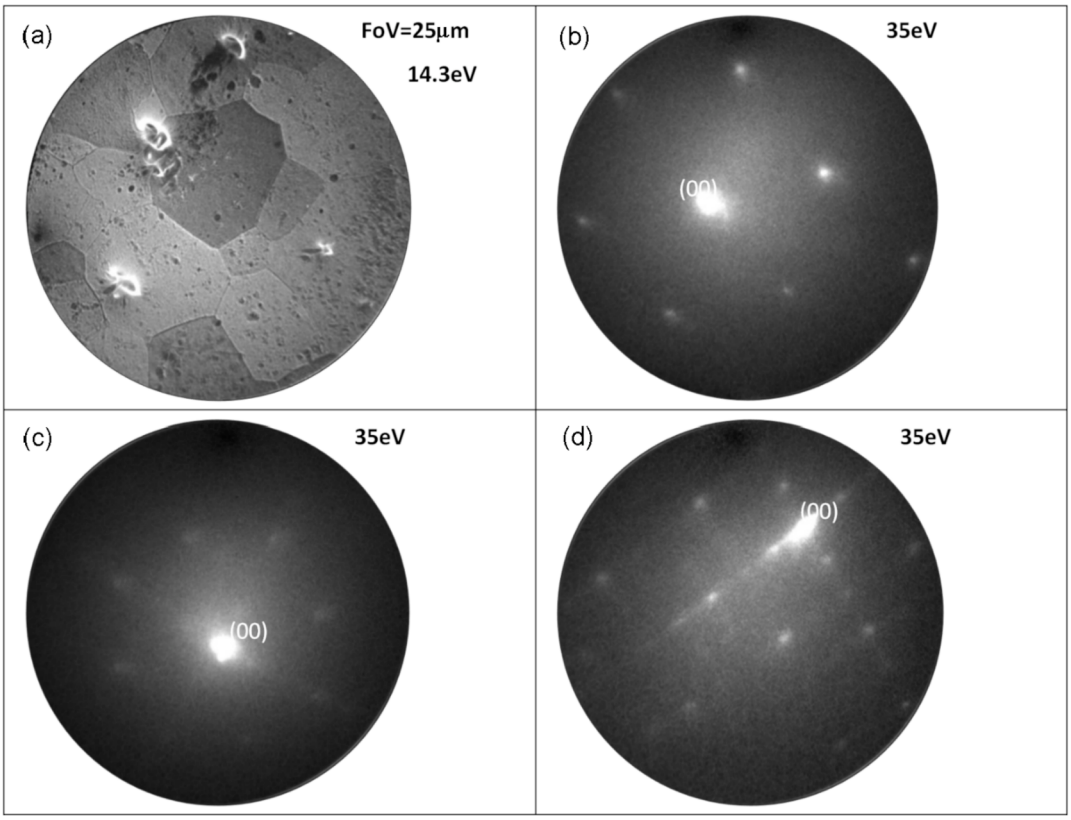

Fig. 5. LEEM image of the polished electrolyte collected at 540 °C, 14.3 eV, FoV = 25 μm (a), b–d) micro-LEED patterns from individual grains acquired at 35 eV (b–d).

surface of the electrolyte is covered by silver particles of up to 500 nm diameter. The similar silver deposit borders are presented in Refs. [3,11]. No changes in the shape or the position of silver particles were noticed. During the cooling cycle, high-quality SEM images were obtained above 275 °C, in other words the specific resistance of the electrolyte was lower than 6 kΩ m^{-1} in this range. FEGSEM images of the border of the silver electrode are shown in Fig. 9.

It can be seen that no influence of temperature change or time was observed on silver movement All visible silver crystallites maintained their size and position. The colour of the electrolyte following this experiment remained unchanged i.e. white.

3.7. The electrical conductivity of CeScSZ samples studied by means of broadband electrochemical impedance spectroscopy before and after the LEEM experiment

The EIS spectra measured at temperatures above 287 °C consist of clearly separated high-frequency (HF), the much smaller medium-frequency (MF) semicircles ascribed to oxygen ion relaxation in grain interior and grain boundaries, respectively, as well as a low-frequency part ascribed to electrode reaction processes (Fig. 10). The spectra in the range 207–287 °C contain only a part of the MF semicircle, whereas at lower temperatures only a part of the HF semicircle is visible.

The equivalent electrical circuits (EECs) used for fitting impedance spectra consist of up to four resistors and capacitor (R, C) parallel pairs connected in series (Fig. 11a). Each capacitor is replaced by a constant phase element (CPE), whose impedance can be expressed by the following formula [29]:

$$Z_{\mathrm{CPE_i}} = \frac{1}{2\pi f_0 C_\mathrm{i}} \left(\frac{f_0}{\mathrm{j}\, f}\right)^{\alpha} \tag{1}$$

where: f is the frequency, f_0 is the frequency of reference usually assumed (f_0 = 1000) Hz [29], j is an imaginary unit, C_i is the capacitance at the frequency of reference, index i is the number of the (R, CPE) pair, and α is a coefficient, with a value ranging between 0.5 and 1. For an ideal capacitor, α is equal to 1, but its values are usually within the range 0.8–1.0 or are close to 0.5 for diffusion processes. An example of fitted spectra is presented in Fig. 11b. The fitted parameters are presented in Table 2 in supporting materials.

The specific grain interior and grain boundary conductivities should rely on temperature (Fig. 12) according to the formula:

$$\log\,(\sigma T) = \frac{-E_A}{2.30258\, k_B} \tag{2}$$

where T is the temperature E_A is activation energy, and k_B is the Boltzmann constant.

The obtained activation energies for grain boundary conductivity is 1.36 eV, whereas the dependency the grain interior conductivity is not a straight line. Obtained activation energies are 1.15, 1.51 and 1.00 eV at 127–247, 267–467 and 487–727 °C, respectively. The slope of this dependency decreases along with increases in temperature; for example within the range 627–727 °C, activation energy is equal to 0.85 eV. The reason for this behaviour is interpreted in terms of defect association or clustering [30]. The temperature dependency for the grain interior conductivity of CeScSZ ceramic, characterised by a similar shape, was reported in Ref. [31].

Comparison of conductivity measurements performed on the

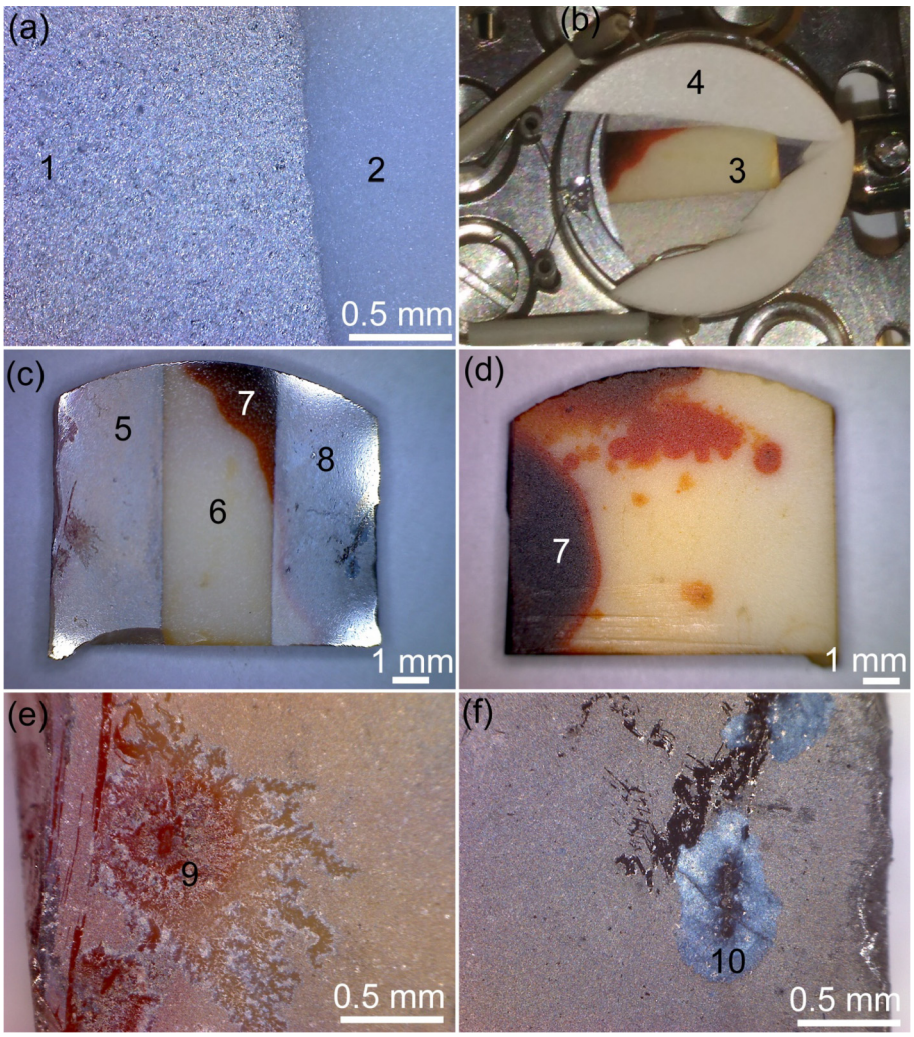

Fig. 6. Images of the cell after 162 min 12 V polarisation at 540 °C in LEEM at 2×10^{-8} mbar. 1 – silver electrode and 2 – electrolyte before LEEM experiment for comparison (a); 3 – the cell in the holder after LEEM experiment, 4 – Al_2O_3 insulator (b); cell: 3 – cathode 6 – electrolyte, 7 – red coloured electrolyte, 8 anode (c); rear side of the cell: 7– red coloured electrolyte (d); 9 – place where the current collector contacted the cathode (e); 10 – the site where the current collector contacted the anode (f).

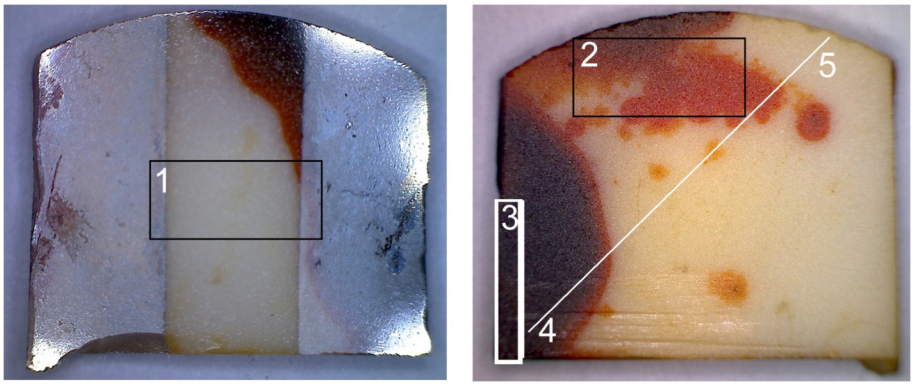

Fig. 7. Places where post-mortem analysis was taken: 1 – an area where SEM examinations of surface change were performed described in section 3.5; 2 – an area where XPS measurements were performed described in section 3.8; 3 – cut-off cuboid for EIS measurements described in section 3,7; 4–5 breaking line for SEM cross-section examination described in section 3.5.

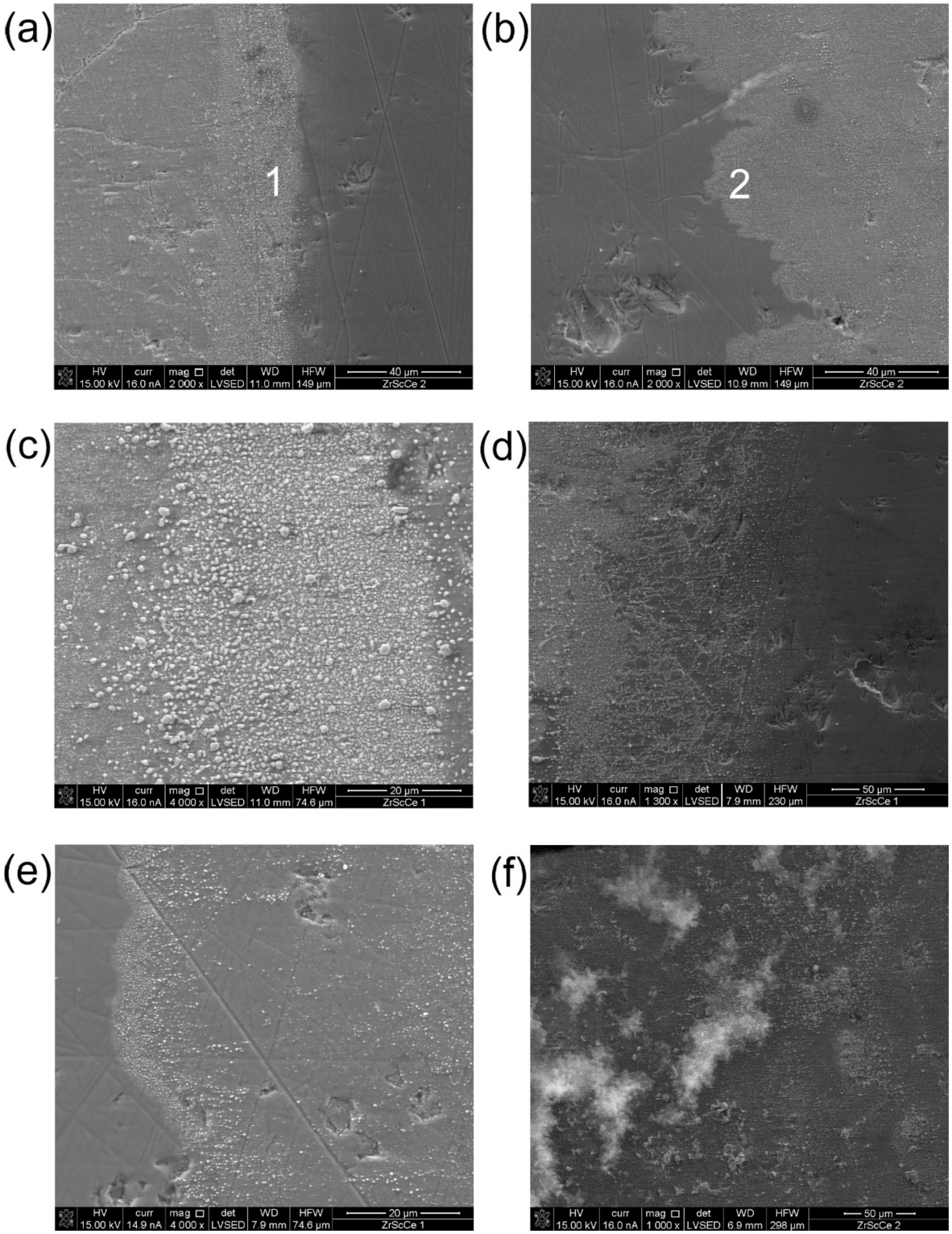

Fig. 8. Microstructure of Ag|CeScSZ|Ag cell after the LEEM experiment: general view of the sample surface along with magnifications of the planar border marked with 1 (a), and the irregular border marked 2 (b); border 1 at higher magnifications (c) and (d); border 2 at higher magnifications (e); electrode surface behind (further to the left of) the border 2.

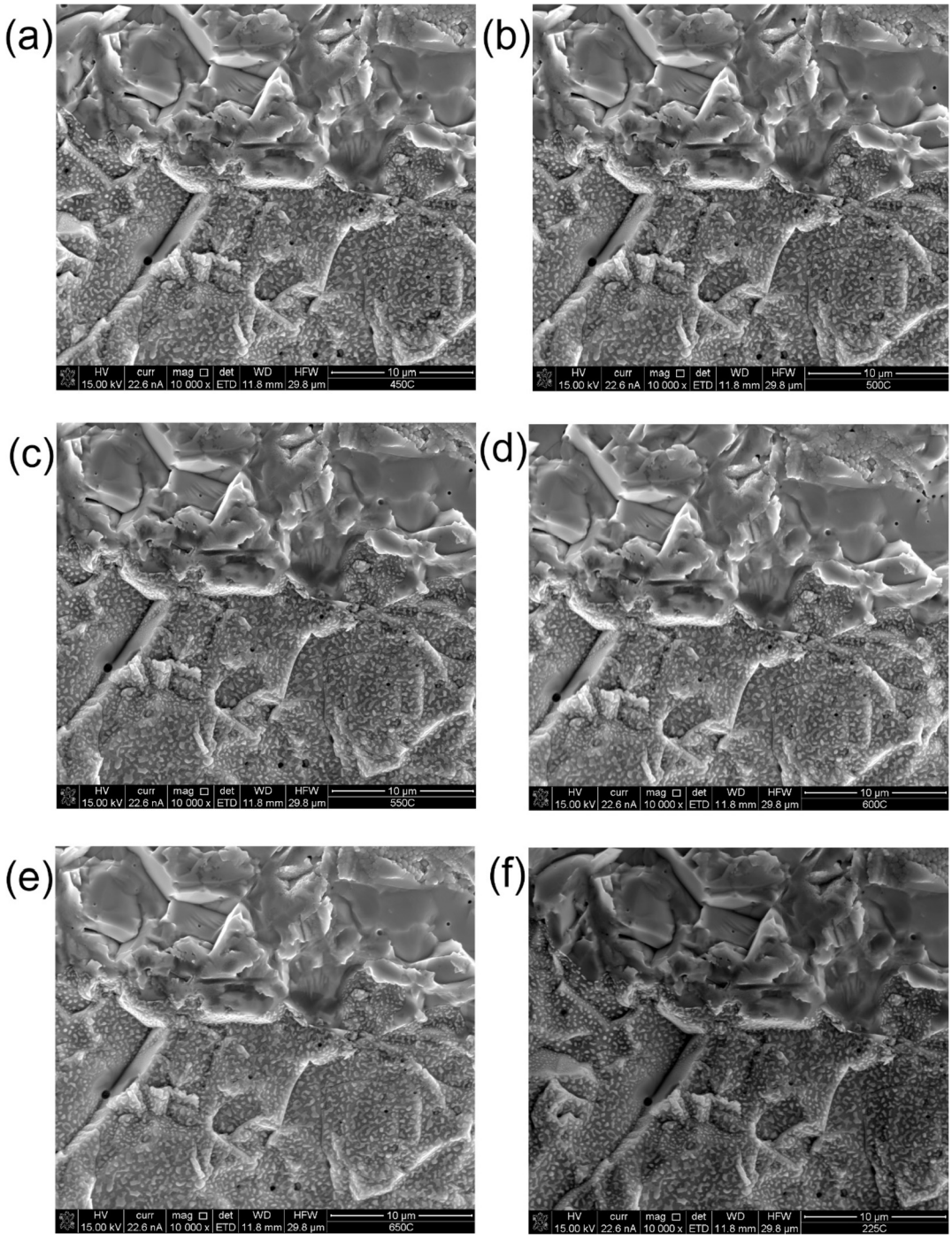

Fig. 9. SEM images of the border of the silver electrode at a) 450, b) 500, c) 550, d) 600, e) 650, f) 225 °C.

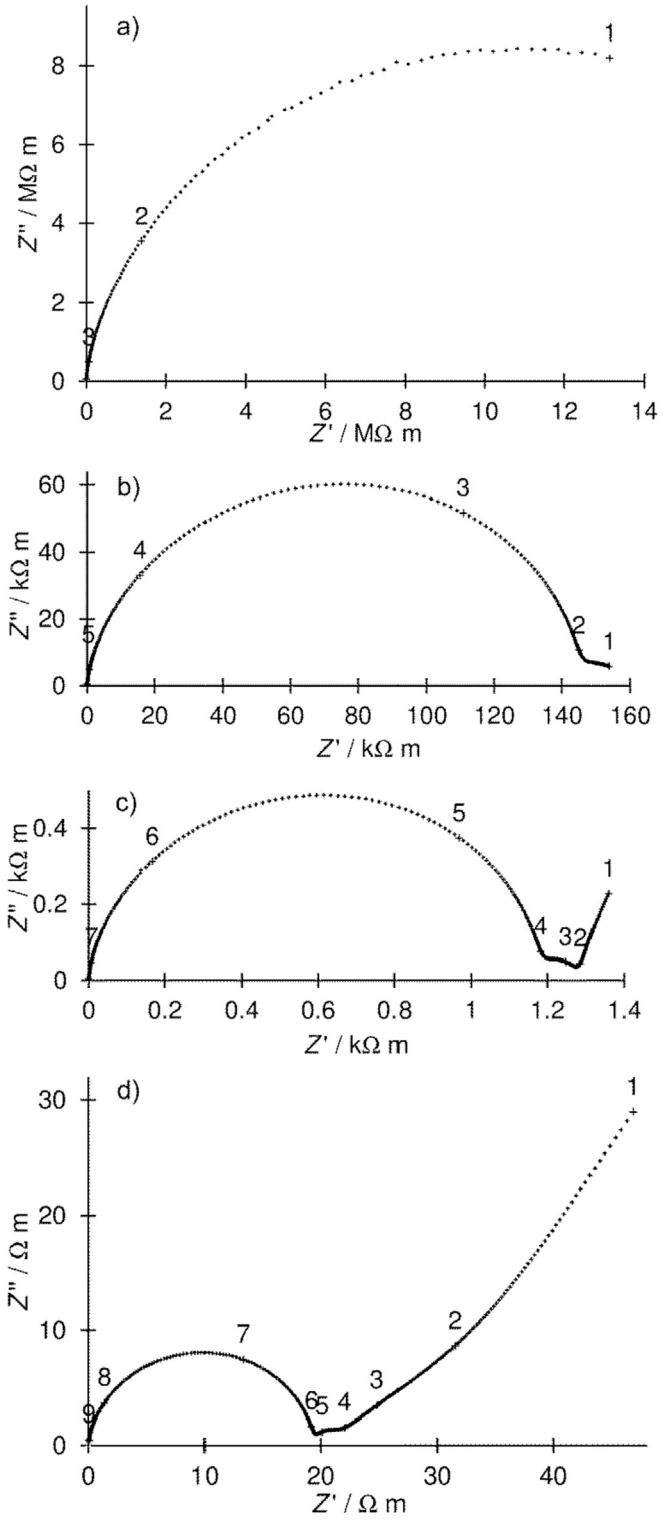

Fig. 10. Examples of EIS spectra in Nyquist representation recorded in air, the numbers above enlarged experimental points denote the logarithm of the frequency: (a) 147, (b) 227, (c) 327, (d) 427 °C.

freshly sintered sample and red part of the sample polarised in LEEM (Fig. 7 the part marked 3) revealed that the presence of silver does not change grain boundary conductivity, however, the bulk conductivity is reduced approximately threefold (Fig. 12).

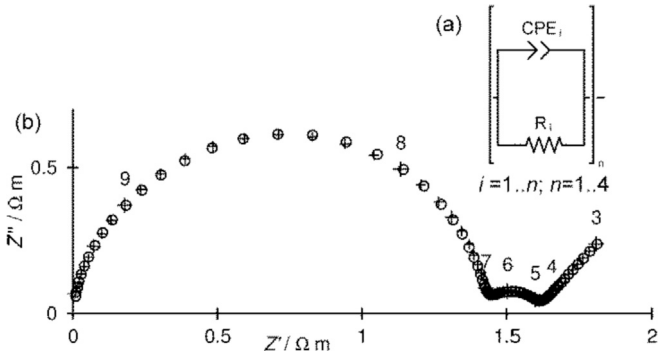

Fig. 11. EECs used for fitting impedance spectra (a); an example of EIS spectra in Nyquist representations in the air at 527 °C; for improved readability, every fifth frequency point is presented; crosses – measured data, circles – fitted data; the numbers above enlarged experimental points denote the logarithm of the frequency (b).

3.8. XPS analyses of the CeScSZ samples before and after the LEEM experiment

3.8.1. Before the experiment

The CeScSZ electrolyte surface was characterised by XPS (Fig. 13). The atomic concentrations of the elements at the studied surface were 52.5% for O, 23.5% for Zr, 1.5% for Ce and 3.5% for Sc. Apart from the main electrolyte components, adsorbed organic carbon (17.8%) and other trace elements (Zn – 0.3%, La – 0.5%, Bi – 0.2%, Pb – 0.3%) were also found. The oxide surface (68% of the total oxygen) was found as covered by hydroxyl groups (23.8% of total oxygen). Analysis of the Zr 3d core excitation spectrum revealed three doublet components assigned to carbides (1.3%), lattice zirconium (IV) oxides (89.2%), and zirconium hydroxides (9.5%) [32]. The Ce 3d spectrum revealed the presence of two cerium (IV) and one cerium (III) states. The spectrum component at BE of 880.6 eV (22.4% of total Ce) was ascribed to the CeO_2 phase on the surface of mixed zirconium oxide similarly to a $CeO_2/(CeO_x + Y_2O_3{+}ZrO_2)$ system [33]. The main component of the Ce 3d spectrum at BE of 884.9 eV (49.0%) was assigned to CeO_2 [32]. The deconvolution also showed the presence of Ce^{3+} ions in the form of Ce_2O_3 oxide [34]. Scandium ions were present in the electrolyte as Sc^{3+} ions in oxide like surrounding [32].

3.8.2. After the experiment

The XPS measurement of the electrolyte surface opposite to surface where electrodes were placed (rectangle 2 in Fig. 7) after polarisation at 530 °C was performed in order to analyse the electronic state of silver. The acquired Ag 3d spectrum is shown in Fig. 14. The deconvolution revealed two doublet components of the spectrum at electron binding energies (BE) of 367.6 eV (A component) and 369.5 eV (B component). The more intensive A component (75.9%) was assigned to Ag–O bonding in Ag_2O lattice [32], and the less intensive B component (24.1%) to Ag^+ in the highly electronegative surroundings. The latter component shows BE similar to $Ag3d_{5/2}$ in $Na_{28.3}Ag_{25.5}Al_{54}Si_{138}O_{184}$ zeolite oxidised at 673 K [35], suggesting interaction of the diffused Ag^+ ions with zirconate lattice leading.

The Ce 3d spectrum acquired at the electrolyte surface after polarisation (Fig. 15) was deconvoluted into multiplet components assigned to Ce(III) and Ce(IV) ions [36]. The deconvolution revealed the surface contains mostly (75%) Ce^{3+} in oxide lattice. Rest of cerium (25%) was present as Ce^{4+} in CeO_2 [32]. The O 1s, Zr 3d and Sc 2p spectra for the polarised electrolyte showed limited differences in the electronic states of the elements at the surface after

Table 2
Values of fitted parameters of the equivalent circuit as a function of temperature.

T/°C	C_1/nF	α_1	C_2/μF	α_2
300	0.27	1.00	–	–
330	0.27	0.99	–	–
360	0.28	0.98	–	–
390	0.29	0.95	–	–
420	0.32	0.91	–	–
450	0.38	0.88	–	–
480	0.47	0.87	–	–
500	0.54	0.87	1.26	1.00
520	0.63	0.87	1.49	1.00
540	0.71	0.87	1.60	0.99
560	0.80	0.87	1.68	1.00
580	0.90	0.87	1.65	1.00
600	1.00	0.87	1.55	0.95
620	1.15	0.87	1.76	0.95
640	1.22	0.87	1.97	0.89
660	1.39	0.87	2.45	0.87
680	1.30	0.89	2.52	0.86
700	1.45	0.88	2.63	0.90
720	1.58	0.88	2.54	0.92
740	1.60	0.89	2.69	0.90
760	1.58	0.89	2.50	0.92
780	1.58	0.89	2.43	0.93
800	1.64	0.89	2.53	0.95
820	1.69	0.89	2.62	0.99
840	1.64	0.90	2.56	0.96
860	1.66	0.90	2.60	0.97
880	1.75	0.90	2.21	1.00
900	1.69	0.90	2.78	0.97
920	1.71	0.90	2.34	1.00
940	1.54	0.91	2.45	0.99
960	1.59	0.90	2.38	1.00
980	1.56	0.91	2.43	1.00
1000	1.53	0.91	2.42	1.00
980	1.41	0.91	2.30	0.99
960	1.48	0.91	2.25	0.99
940	1.62	0.90	2.23	1.00
920	1.64	0.90	2.17	1.00
900	1.67	0.90	2.09	1.00
880	1.68	0.90	2.00	1.00
860	1.66	0.90	1.90	1.00
840	1.65	0.90	1.86	0.99
820	1.58	0.90	2.10	0.96
800	1.72	0.89	1.99	0.96
780	1.60	0.89	2.76	0.89
760	1.67	0.89	2.10	0.95
740	1.51	0.89	2.45	0.96
720	1.58	0.88	4.07	0.90
700	1.53	0.88	2.37	0.95
680	1.50	0.87	2.12	1.00
660	1.43	0.87	1.82	1.00
640	1.22	0.87	1.46	1.00
620	1.02	0.88	1.16	0.93
600	1.00	0.87	1.20	1.00
580	0.92	0.86	1.40	1.00
560	0.81	0.86	1.28	1.00
540	0.71	0.87	1.25	1.00
520	0.63	0.86	1.03	1.00
500	0.55	0.87	0.70	0.96
480	0.47	0.86	0.93	1.00
460	0.40	0.87	–	–
440	0.55	0.91	–	–
420	0.52	0.95	–	–
400	0.40	0.99	–	–

polarisation.

XRD investigations performed on the CeScSZ samples after polarisation confirmed the presence of metallic silver particles (111) and (002) on the CeScSZ surfaces.

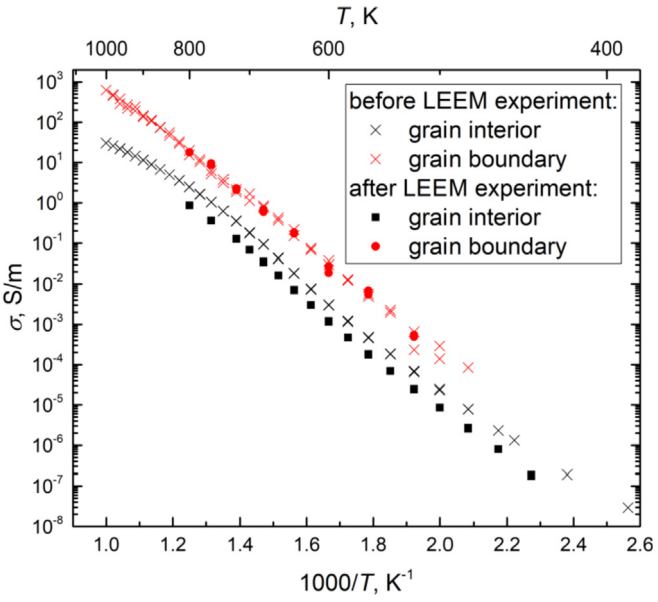

Fig. 12. Arrhenius plot of grain interior (black) and grain boundary (red) conductivity of CeScSZ before (× , ✕) and after (■, ●) the LEEM experiment.

3.9. Proposed mechanism of silver migration based on the results of XPS, SEM, FEGSEM, LEEM, and EIS

The described observations of oxygen pressure in the LEEM microscope chamber during the electrochemical experiment and postmortem analysis of the cell using the EIS, SEM, FEGSEM, XPS, and XRD methods can be explained in terms of the following electrochemical reactions.

During polarisation, due to the oxidation process at the anode, gaseous oxygen is evolved:

$$2O^{2-} \rightleftarrows O_2 + 4e^- \quad (3)$$

Thus increasing the gas pressure in the microscope chamber. At the same time, the reduction process must take place at the cathode in order to keep the solid sample electrically unloaded. The potential reaction:

$$Ag + e^- + V_O^{\cdot\cdot} \rightleftarrows Ag_O^{\cdot} \quad (4)$$

followed by the movement of $Ag_O^{\bullet}$ from one site to another through oxygen vacancies to the anode is a possible reason for the presence of silver inside the electrolyte on the anode side. The significant decrease in the grain interior ionic conductivity of the CeScSZ electrolyte may be caused by a reduction in the concentration of unoccupied oxygen vacancies. The presence of silver on the opposite side of the electrolyte disc is confirmed by EDS, XPS, and XRD.

3.10. The ceria reduction process

$$Ce^{+4} + e^- \rightleftarrows Ce^{3+} \quad (5)$$

May also take place at the anode; however, the concentration of ceria ions in the cationic net is too low to cause such a large decrease in ionic grain interior conductivity.

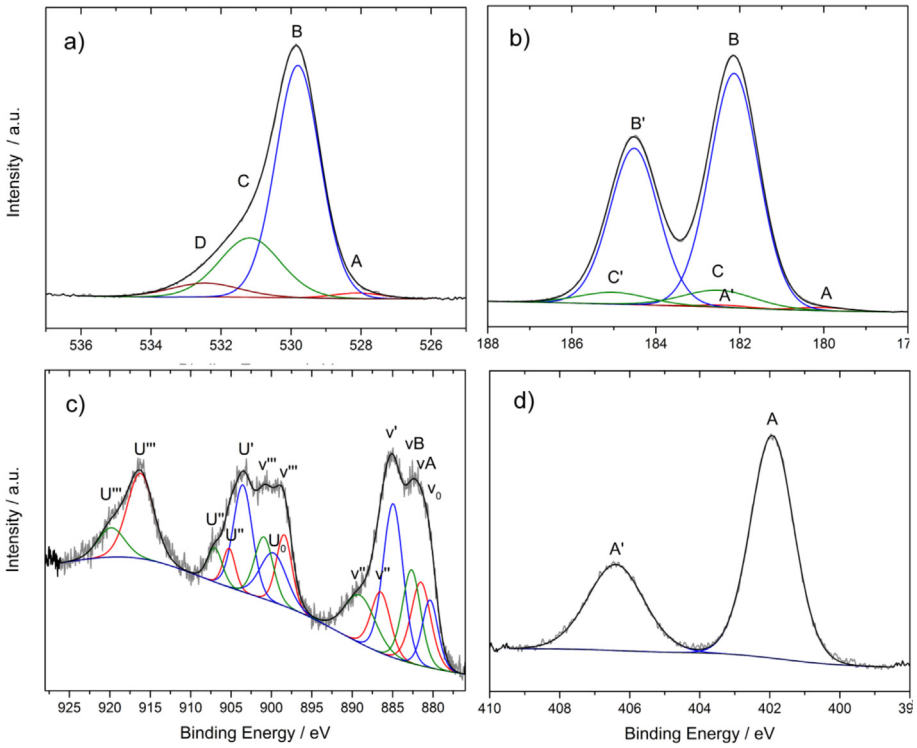

Fig. 13. The deconvoluted high-resolution spectra of O 1s (a), Zr 3d (b), Ce 3d (c), and Sc 2p (d) core excitations.

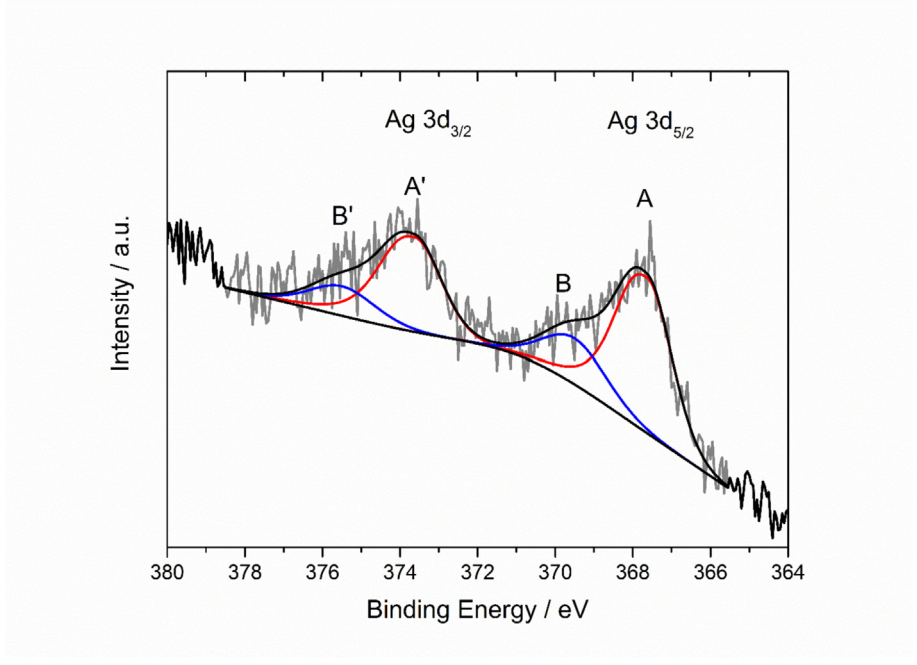

Fig. 14. Deconvolution of Ag 3d core excitation acquired at the electrolyte surface.

4. Conclusions

Examination of the polarised Ag|CeScSZ|Ag cell in situ in LEEM did not permit observation of the movement of silver particles; however, post-mortem observations using optical and scanning electron microscopes showed huge changes in the morphology of silver electrodes and electrolyte.

High temperature in situ FEGSEM examinations of the reference

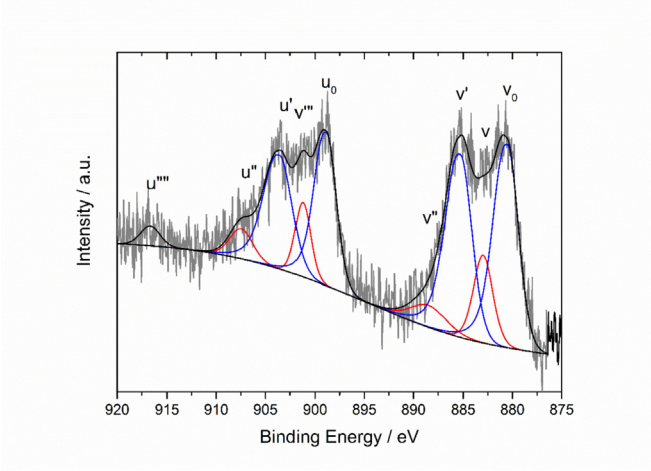

Fig. 15. The deconvolution of Ce 3d core excitation acquired at electrolyte surface after polarisation.

cell showed that the morphology of the cathode and isolated silver particles remained unchanged during heating and cooling without polarisation.

A new potential mechanism of silver migration through the bulk of crystal grains of CeScSZ is proposed, assuming the migration of Ag^{-} ions through oxygen ion vacancies. This process reduces the ionic bulk conductivity of the CeScSZ electrolyte.

Author statement

M. Mosiałek: Conceptualization, Methodology, Software, Validation, Formal analysis, Investigation, Resources, Data Curation, Writing - Original Draft, Writing - Review & Editing, Visualization, Supervision, Project administration; R.P. Socha: Conceptualization, Writing - Review & Editing, Concerning XPS: Formal analysis, Investigation, Data Curation, Writing - Original Draft, Visualization. B. Bożek; Concerning XRD, Rietfeld: Methodology, Data Curation, Formal analysis, Validation, Investigation, Writing - Original Draft, Writing - Review & Editing, Visualization, D. Wilgocka-Ślęzak Concerning LEEM: Methodology, Investigation, Data Curation, Writing - Original Draft, Writing Review & Editing, Visualization, E. Bielańska: Concerning SEM: Investigation, Data Curation, Writing - Original Draft, A. Kežionis: Methodology: Development or design of methodology; creation of models Software: Programming, software development; designing computer programs; implementation of the computer code and supporting algorithms; testing of existing code components T. Šalkus: Investigation: Conducting a research and investigation process, specifically performing the experiments, or data/evidence collection. Visualization: Preparation, creation and/or presentation of the published work, specifically visualization/data presentation. E. Kazakevičius: Investigation: Conducting a research and investigation process, specifically performing the experiments, or data/evidence collection. A.F. Orliukas: Methodology: Development or design of methodology; creation of models. M. Dziubaniuk: Concerning electrolyte disks: Methodology, Investigation, Data Curation, Writing - Original Draft, J. Wyrwa: Concerning electrolyte disks: Methodology, Investigation, Data Curation, Writing - Original Draft, J. Wojewoda-Budka: Concerning SEM: Investigation, Data Curation, Visualization, Writing - Original Draft, Writing – Review & Editing, M. Faryna Low-vacuum and high-resolution scanning electron microscopy investigations B. Lis Concerning: electrolyte disks: Methodology, Investigation, Data Curation, Visualization. M. Dudek: Writing - Review & Editing, Concerning electrolyte disks and XRD: Methodology, Investigation, Validation, Data Curation, Visualization. R. Lach Concerning XRD, Rietfeld: Methodology, Investigation, Validation, Data Curation, Formal analysis, Visualization.

Acknowledgments

The European Union Erasmus + programme (project number: 2015-1-PL01-KA103-014791) is acknowledged for providing scholarship (financial support) for the research/mobility/traineeship. Some measurements were performed using scientific equipment belonging to the laboratories of the AGH-UST Energy Centre, Cracow, Poland.

References

[1] D.H. Kim, K. Bae, H.J. Choi, J.H. Shim, Ag surface-coated with nano-YSZ as an alternative to Pt catalyst for low-temperature solid oxide fuel cells, J. Alloy, Compd 769 (2018) 545.
[2] M. Mosiałek, A. Michna, M. Dziubaniuk, E. Bielańska, A. Kežionis, T. Šalkus, E. Kazakevičius, B. Bożek, A. Krawczyk, J. Wyrwa, A.F. Orliukas, Composite cathode material LSCF-Ag for solid oxide fuel cells obtained in one step sintering procedure, Electrochim. Acta 282 (2018) 427.
[3] M. Mosiałek, M. Dudek, J. Wojewoda-Budka, Composite $La_{0.6}Sr_{0.4}Co_{0.8}Fe_{0.2}O_3$/Ag cathode for SOFCs with $Ce_{0.8}Sm_{0.2}O_{1.9}$ electrolyte, Arch. Metall. Mater. 58 (2013) 275.
[4] K. Sasaki, M. Muranaka, T. Terai, Compatibility analysis of Ag and electrolyte materials for LT-SOFCs and LT-SOECs, Solid State Ionics 181 (2010) 1303.
[5] A. Jaiswal, E. Wachsman, Direct current bias studies on $(Bi_2O_3)_{0.8}(Er_2O_3)_{0.2}$ electrolyte and Ag–$(Bi_2O_3)_{0.8}(Er_2O_3)_{0.2}$ cermet electrode, Solid State Ionics 177 (2006) 677.
[6] M. Camaratta, E. Wachsman, Silver–bismuth oxide cathodes for IT-SOFCs; Part I – microstructural instability, Solid State Ionics 178 (2007) 1242.
[7] M. Camaratta, E. Wachsman, Silver–bismuth oxide cathodes for IT-SOFCs: Part II – improving stability through microstructural control, Solid State Ionics 178 (2007) 1411.
[8] J. Nielsen, T. Jacobsen, Three-Phase-Boundary dynamics at metal/YSZ microelectrodes, Solid State Ionics 178 (2008) 1769.
[9] A. Razniak, M. Dudek, P. Tomczyk, Reduction of oxygen at the interface M|solid oxide electrolyte (M=Pt, Ag and Au, solid oxide electrolyte=YSZ and GDC). Autocatalysis or artifact? Catal. Today 176 (2011) 41.
[10] M. Mosiałek, E. Bielańska, R.P. Socha, M. Dudek, G. Mordarski, P. Nowak, J. Barbasz, A. Rapacz-Kmita, Changes in the morphology and the composition of the Ag|YSZ and Ag|LSM interfaces caused by polarization, Solid State Ionics 225 (2012) 755.
[11] M. Mosiałek, M. Dudek, P. Nowak, R.P. Socha, G. Mordarski, E. Bielańska, Changes in the morphology and the composition of the Ag|$Gd_{0.2}Ce_{0.8}O_{1.9}$ interface caused by polarization, Electrochim. Acta 104 (2013) 474.
[12] M. Dudek, M. Mosiałek, P. Nowak, J. Wojewoda-Budka, M. Reben, Silver migration at the Ag|$Sm_{0.2}Ce_{0.8}O_{1.9}$ interface, J. Solid State Electrochem. 18 (2014) 2529.
[13] J. Nielsen, T. Jacobsen, Three-phase-boundary dynamics at Pt/YSZ microelectrodes, Solid State Ionics 178 (2007) 1001.
[14] P. Tomczyk, S. Żurek, M. Mosiałek, Effect of time and polarization on kinetics of the oxygen electrode reaction at an Au|YSZ interface, J. Electroceram. 23 (2009) 25.
[15] H.R. Choi, K.C. Neoh, H.J. Choi, G.D. Han, J.H. Shim, Nanoporous silver cathode surface-treated by aerosol-assisted chemical vapor deposition of gadolinia-doped ceria for intermediate-temperature solid oxide fuel cells, J. Power Sources 402 (2018) 246.
[16] S.V. Seyed-Vakili, A. Babaei, M. Ataie, S. Heshmati-Manesh, H. Abdizadeh, Enhanced performance of $La_{0.8}Sr_{0.2}MnO_3$ cathode for solid oxide fuel cells by co-infiltration of metal and ceramic precursors, J. Alloys Compd. 737 (2018) 43.
[17] Z.G. Lu, J.H. Zhu, Thermal evaporation of pure Ag in SOFC-relevant environments, Electrochem. Solid State Lett. 10 (2007) B179.
[18] P.S. Ho, H.B. Huntington, Electromigration and void observation in silver, J. Phys. Chem. Solid. 27 (1966) 1319.
[19] S.P.S. Badwal, F.T. Ciacchi, D. Milosevic, Scandia–zirconia electrolytes for intermediate temperature solid oxide fuel cell operation, Solid State Ionics 136–137 (2000) 91.
[20] S. Kazlauskas, A. Kežionis, E. Kazakevičius, A.F. Orliukas, Charge carrier relaxation and phase transition in scandium stabilized zirconia ceramics, Electrochim. Acta 134 (2014) 176.
[21] H. Tu, X. Liu, Q. Yu, Synthesis and characterization of scandia ceria stabilized zirconia powders prepared by polymeric precursor method for integration into anode-supported solid oxide fuel cells, J. Power Sources 196 (2011) 3109.
[22] M.A. Laguna-Bercero, S.J. Skinner, J.A. Kilner, Performance of solid oxide electrolysis cells based on scandia stabilised zirconia, J. Power Sources 192

(2009) 126.
[23] J.H. Joo, G.M. Choi, Electrical conductivity of scandia-stabilized zirconia thin film, Solid State Ionics 179 (2008) 1209.
[24] H.A. Abbas, C. Argirusis, M. Kilo, H.-D. Wiemhöfer, F.F. Hammad, Z.M. Hanafi, Preparation and conductivity of ternary scandia-stabilised zirconia, Solid State Ionics 184 (2011) 6.
[25] H.P. Dasari, J.S. Ahn, K. Ahn, S.-Y. Park, J. Hong, H. Kim, K.J. Yoon, J.-W. Son, H.-W. Lee, J.-H. Lee, Synthesis, Sintering and conductivity behavior of ceria-doped Scandia-stabilized zirconia, Solid State Ionics 263 (2014) 103.
[26] V. Petříček, M. Dušek, L. Palatinus, Crystallographic computing system JANA2006: general features, Z. Kristallogr. 229 (2014) 345.
[27] A. Kežionis, E. Kazakevičius, T. Šalkus, A. Orliukas, Broadband high frequency impedance spectrometer with working temperatures up to 1200K, Solid State Ionics 188 (2011) 110.
[28] F. James, M. Roos, Minuit a system for function minimalization and analysis of the parameter errors and correlations, Comput. Phys. Commun. 10 (1975) 343.
[29] M. Mosiałek, P. Nowak, M. Dudek, G. Mordarski, Oxygen reduction at the silver|$Gd_{0.2}Ce_{0.8}O_{1.9}$ interface studied by electrochemical impedance spectroscopy and cyclic voltammetry at the silver point electrode, Electrochim. Acta 120 (2014) 248.
[30] W. Preis, J. Waldhäusl, A. Egger, W. Sitte, E. de Carvalho, J.T.S. Irvine, Electrical properties of bulk and grain boundaries of scandia-stabilized zirconia co-doped with yttria and ceria, Solid State Ionics 192 (2011) 148.
[31] S. Kazlauskas, E. Kazakevičius, A. Kežionis, Electrical properties of scandia- and ceria-stabilized zirconia ceramics, Solid State Ionics 310 (2017) 143.
[32] NIST X-Ray Photoelectron Spectroscopy Database, National Institute of Standards and Technology, Gaithersburg, 2012, Version 4.1. http://srdata.nist.gov/xps/.
[33] G.M. Ingo, E. Paparazzo, O. Bagnarelli, N. Zacchetti, XPS studies on cerium, zirconium and yttrium valence states in plasma-sprayed coatings, Surf. Interface Anal. 16 (1990) 515.
[34] A. Pfau, K.D. Schierbaum, The electronic structure of stoichiometric and reduced CeO_2 surfaces: an XPS, UPS and HREELS study, Surf. Sci. 321 (1994) 71.
[35] W. Grunert, R. Schlogl, H.G. Karge, Photoelectron and ion-scattering spectroscopy of zeolites under reduced surface-charge conditions, J. Phys. Chem. 97 (1993) 8638.
[36] E. Beche, P. Charvin, D. Perarnau, S. Abanades, G. Flamant, Ce 3d XPS investigation of cerium oxides and mixed cerium oxide ($Ce_xTi_yO_z$), Surf. Interface Anal. 40 (2008) 264.